Simulation of Semiconductor Processes and Devices 2016
Edited by E. Bär, J. Lorenz, and P. Pichler

A Self-Consistent Solution of the Poisson and Boltzmann Equations for Electrons in Graphene with a Deterministic Approach

Oliver Dieball*, Zeinab Kargar, Dino Ruić and Christoph Jungemann
Chair of Electromagnetic Theory
RWTH Aachen University
52056 Aachen, Germany
*Email: oliver.dieball@rwth-aachen.de

***Abstract*—We present the first deterministic approach for solving the Poisson and Boltzmann equations for electrons in graphene based on the expansion of the Boltzmann equation in Fourier harmonics and a Gummel iteration scheme. The approach is applied to a double-gate graphene field effect transistor considering anisotropic scattering by acoustic and optical phonons as well as remote phonons, emerging from the gate oxide. Results are presented which show the device characteristics and the feasibility of our simulator.**

I. Introduction

Since the discovery of graphene, which was awarded with the Nobel Prize [1], a great amount of work has been put into the research of its properties, e.g. by Graphene Flagship [2]. To receive a detailed picture about the electronic properties of a device that uses graphene a precise modeling of the band structure and scattering mechanisms must be possible. The deterministic solution of the Boltzmann equation (BE) based on an expansion of $\mathbf{k}$-space into Fourier harmonics appears to be a reasonable approach [3]. It has unique advantages compared to the Monte Carlo approach, e.g. no stochastic errors and the possibility to perform small-signal analysis [4]. For silicon and GaAs devices deterministic solvers of the BE with a Fourier harmonics expansion of $\mathbf{k}$-space have been developed successfully in Refs. [5] and [6], respectively. In graphene devices the major differences are the true 2D channel, the band structure and the scattering mechanisms which suppress back-scattering [7]. A Monte Carlo BE solver for graphene considering anisotropic scattering has been demonstrated in Ref. [8].

In this work we present a self-consistent deterministic solver for the coupled system of Poisson equation (PE) and BE for a double-gate graphene field effect transistor (DGFET).

II. Simulation Approach

We consider the device shown in Fig. 1. It is assumed to be translational invariant in z-direction. The BE is solved one-dimensionally in y-direction (transport direction) and the PE is solved two-dimensionally in the x-y-plane. In the following

978-1-5090-0818-6/16/$31.00

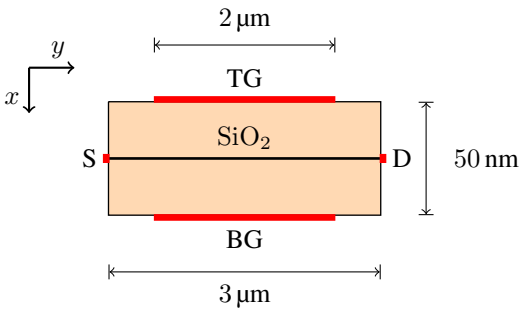

Fig. 1. Double gate graphene FET with SiO_2 as insulator. The red areas indicate the contact areas.

we will show how to set up the equations for the BE and PE.

A. The Boltzmann Equation

The stationary BE is solved for electrons in two-dimensional $\mathbf{k}$-space and one-dimensional transport in real space:

$$F_{\mathrm{BE}} := \frac{1}{\hbar}F_y(y)\frac{\partial}{\partial k_y}f^\nu(y,\mathbf{k}) + v_f\frac{\partial}{\partial y}f^\nu(y,\mathbf{k}) - S^\nu\{f\} = 0,$$

with $f^\nu(y,\mathbf{k})$ the distribution function, ν the valley, $F_y = q\frac{\partial V(x_0,y)}{\partial y}$ the force, x_0 the spatial coordinate of graphene, v_f the group velocity in transport direction and $S^\nu\{f\}$ the scattering integral. Both contacts are implemented by a generation/recombination rate proportional to a recombination velocity [9] which is added to the BE at the source and drain contact grid points.

The kinetic energy is treated as a classical quantity arising from a valley model. The potential energy is obtained from the solution of the PE by $-qV(x,y)$ with q the positive electron charge and $V(x,y)$ the electrostatic potential. The total electron energy is then the sum of both energies.

The conduction band of graphene has its minima at the six Dirac points named $\mathbf{K}$ and $\mathbf{K}'$ as shown left in Fig. 2. For

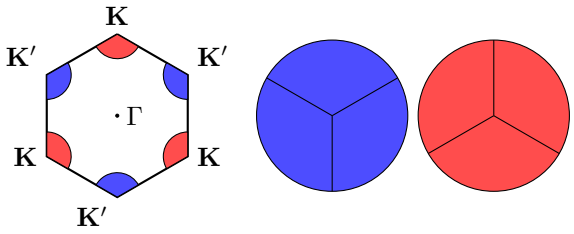

Fig. 2. Left: First Brillouin zone of graphene with the six Dirac points that lie at $\mathbf{K}$ and $\mathbf{K}'$. Right: The linear sections are grouped together into two degenerate valleys with the minimum energy at the origin of the new coordinate system.

the expansion of the $\mathbf{k}$-space into Fourier harmonics a valley model with the minimum energy at the origin of the coordinate system is required [4]. We approximate the band structure in the vicinity of the six Dirac points which yields

$$E(\mathbf{k}) = +\hbar v_\mathrm{f}|\mathbf{k}|,$$

where $v_\mathrm{f} = 8.8 \cdot 10^5\,\mathrm{m\,s^{-1}}$ is the Fermi velocity. The linear sections are grouped into two degenerate valleys, which is shown on the right of Fig. 2.

The H-Transformation [3] and an expansion into Fourier harmonics [4] as well as a projection onto equi-energy surfaces is applied. The Fourier expansion is truncated at an order consistent with the desired precision.

We use the box-integration in real space and energy space to obtain a set of equations, which are derived in Refs. [4], [5]. It should be noted that considering the Pauli principle leads to a non-linear system of equations due to the scattering term.

We consider acoustic [10], optical [11] (PH) and remote phonons [12] (RP) emerging from the gate oxide. In an effective mass approximation the electronic states of graphene near the Dirac points are described by the 2D Dirac equation. This leads to two-component wave functions which are mathematically equivalent to spinors [13]. From this it can be derived that back-scattering is suppressed [14]. We therefore included an anisotropic term in the transition coefficient of all scattering mechanisms

$$C_{\mathbf{k},\mathbf{k}'} = \frac{1+\cos(\theta)}{2}, \tag{1}$$

where θ is the angle between the initial and final wave vector. The inclusion of the anisotropic scattering mechanisms led to similar difficulties as for the simulation of GaAs [6]. The scattering term $S^\nu\{f\}$ is given by the single particle scattering integral:

$$S^\nu\{f\} = \frac{1}{(2\pi)^2}\sum_{\nu',\eta,\sigma}\int\Big\{(1-f^\nu(y,\mathbf{k}))S^{\nu,\nu'}_{\eta,\sigma}(y,\mathbf{k},\mathbf{k}') \times f^{\nu'}(y,\mathbf{k}') - (1-f^{\nu'}(y,\mathbf{k}'))S^{\nu',\nu}_{\eta,-\sigma}(y,\mathbf{k}',\mathbf{k})f^\nu(y,\mathbf{k})\Big\}d^2k', \tag{2}$$

where $S^{\nu,\nu'}_{\eta,\sigma}(y,\mathbf{k},\mathbf{k}')$ is the transition rate containing the anisotropic scattering matrix element, η is the type of scattering and $\sigma = \pm\hbar\omega_\eta$ is the energy transfer. The projection of the scattering term onto Fourier harmonics and equi-energy lines is calculated as [4]

$$S^\nu(y,\tilde{\varepsilon}) = \frac{1}{(2\pi)^2}\int S^\nu\{f\}\delta(\tilde{\varepsilon}-\tilde{\varepsilon}^\nu(y,\mathbf{k}))Y_m(\varphi)d^2k, \tag{3}$$

where $S^\nu\{f\}$ is the single particle scattering integral. The transition rate $S^{\nu,\nu'}_{\eta,\sigma}$ is given by

$$S^{\nu,\nu'}_{\eta,\sigma}(y,\mathbf{k},\mathbf{k}') = c^{\nu,\nu'}_{\eta,\sigma}(y,\mathbf{k},\mathbf{k}')\delta(\varepsilon^\nu(\mathbf{k})-\varepsilon^{\nu'}(\mathbf{k}')-\sigma).$$

For RP the transition coefficient can be expressed as [12]

$$c^{\nu,\nu'}_{\eta=\mathrm{RP},\sigma}(\mathbf{k},\mathbf{k}') = \gamma_0\frac{C_{\mathbf{k},\mathbf{k}'}}{|\mathbf{k},\mathbf{k}'|},$$

where γ_0 contains all constants and the wave vector $|\mathbf{k},\mathbf{k}'|$ is given by

$$|\mathbf{k},\mathbf{k}'|^2 = k^2 + k'^2 - 2kk'\cos(\theta).$$

Because the transition depends on the angle between initial and final wave vector higher harmonic orders have to be considered.

B. The Poisson Equation

Neglecting holes, the PE reads

$$F^\mathrm{PE} := \nabla\cdot[\varepsilon\nabla V(x,y)] + q[n(x,y)-N_\mathrm{i}] = 0,$$

with $n(x,y)$ the electron density, N_i is the intrinsic electron concentration in graphene and ε the dielectric constant. The discretization by box-integration yields a set of equations as in Ref. [5]. The electron density n_inv can be calculated by the zeroth moment of the distribution function

$$n_\mathrm{inv}(y) = 2\sqrt{2\pi}\sum_\nu\int dH\,Z^\nu(H)f^\nu_{m=0}(y,H)$$

where $Z^\nu(H)$ is the density of states. The electron density is used to couple the PE with the BE in the Gummel iteration. The BE is coupled with the PE by the force $F_y(y)$.

III. Results

The results are presented for a DGFET as shown in Fig. 1. To compute the potential and the distribution function the PE and BE are solved with a Gummel iteration method [15] until self-consistency is reached. We consider 33 grid points in real space for the BE and choose the H-grid spacing to be $5.648\,\mathrm{meV}$ which is about $1/26$ of the optical phonon energy. Moreover, we truncate the expansion into Fourier harmonics above the fifth order since no significant change in the drain current was observed. We can show that the resulting set of equations for the BE up to first harmonic order is well behaved and no instabilities occurred during the simulation even for higher orders. The computation of an operating point on a machine with 24 cores takes approximately one hour.

The low-field mobility versus inversion density is shown in Fig. 3 for a system homogeneous in y-direction. The calculations are performed for the intrinsic phonons, PH only

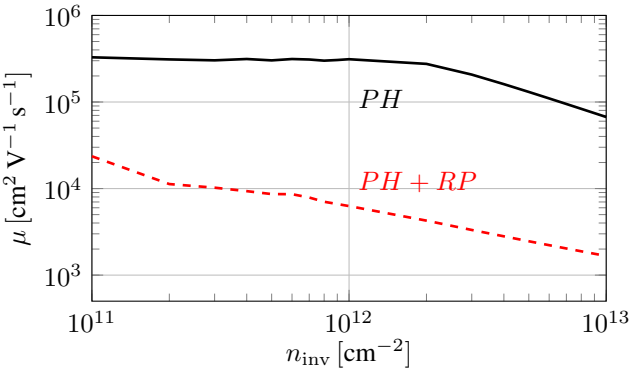

Fig. 3. The mobility μ vs. inversion density n_{inv} considering the intrinsic phonons (solid line) and the remote phonons (dashed). Depending on the choice of gate oxide, the remote phonons can have a major influence.

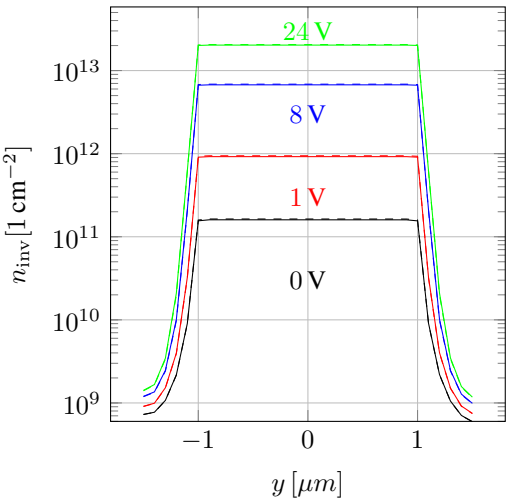

Fig. 4. Inversion density n_{inv} in transport direction for different gate bias V_{TGS} considering the Pauli principle (solid lines) and without (dashed lines).

and as well as with the remote phonons, PH+RP. First, one should notice the high mobility for a low inversion density when only PH is considered. Second, it can be seen that when RP are included the mobility is seriously degraded.

The electron densities for $V_{\mathrm{DS}} = 10\,\mathrm{mV}$ and different gate bias V_{TGS} are shown in Fig. 4 for the transistor. The resulting drain current I_{D} vs. drain voltage V_{DS} for different gate bias V_{TGS} is shown in Fig. 5 with Pauli principle (solid lines) and without (dashed lines). The Pauli principle does not have a significant influence. The drain current I_{D} vs. V_{TGS} for different drain bias V_{DS} is shown in Fig. 6.

The distribution function in $\mathbf{k}$-space is shown in Fig. 7 for a system homogeneous in y-direction at a low and a high field applied in transport direction. It can be seen that the occupation close to equilibrium is low. Far away from equilibrium the maximum value of the occupation is lower and the circle is blurred and shifted in transport direction. Thus, at high bias conditions the device enters ballistic transport which can not be simulated by the drift-diffusion model. Also this indicates that the Pauli principle, which is included in the scattering integral by the $(1 - f^{\nu}(y, \mathbf{k}))$ term, does not have

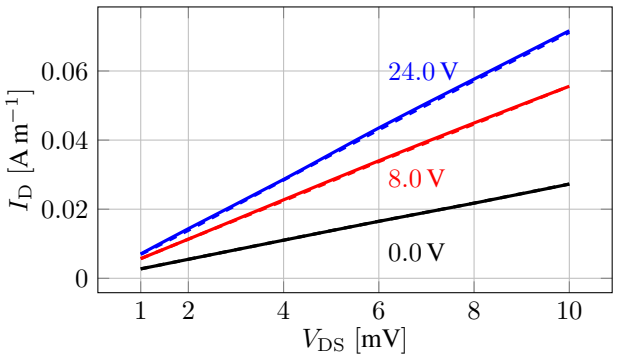

Fig. 5. I_{D} vs. V_{DS} for different applied voltages V_{TGS} considering the Pauli principle (solid lines) and without (dashed lines).

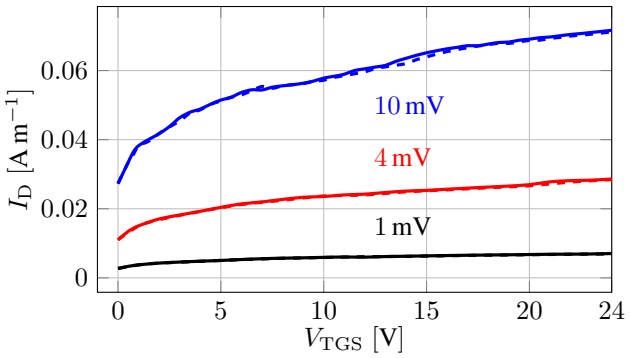

Fig. 6. I_{D} vs. V_{TGS} for different applied voltages V_{DS} considering the Pauli principle (solid lines) and without (dashed lines).

a great influence. The influence of the anisotropic transition rate can be understood when considering the second term (out scattering) of the single particle scattering integral in Eq. (2). The rate $\bar{S}$ considers the scattering of an electron from a state $\mathbf{k}$ with the energy $\tilde{\varepsilon}$ pointing in transport direction ($\phi = 0$) into all other possible states $\mathbf{k}'$ with angle θ for RP close to equilibrium. In Fig. 8 the case of an absorption is shown. The density of states is proportional to the kinetic energy and thus a maximum occurs due to the $Z(H)f(H)$ term in the transformed scattering integral. The case of an emission is shown in Fig. 9. The scattering rate starts to increase from the phonon energy and again reaches a maximum. Thus, because of this energy dependence the correct scattering rates can only be obtained if the correct distribution function for the ballistic transport can be computed. In both cases the back-scattering is suppressed.

IV. Conclusion

We have presented the first deterministic solver for electrons in a graphene device based on an expansion into Fourier harmonics including the Pauli principle and anisotropic scattering mechanisms. Our approach for the simulator is stable for a large range of bias conditions. The results show a major influence of RP on the mobility and indicate the importance of a Boltzmann equation based model for transport.

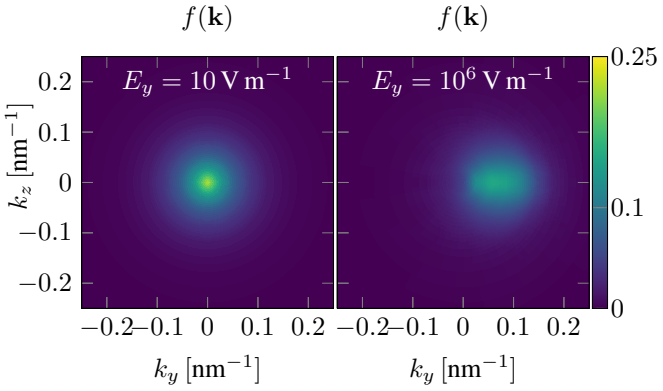

Fig. 7. Distribution function in **k**-space for a low and high field applied in transport direction. The occupation is low in both cases indicating that the Pauli principle does not have a great influence.

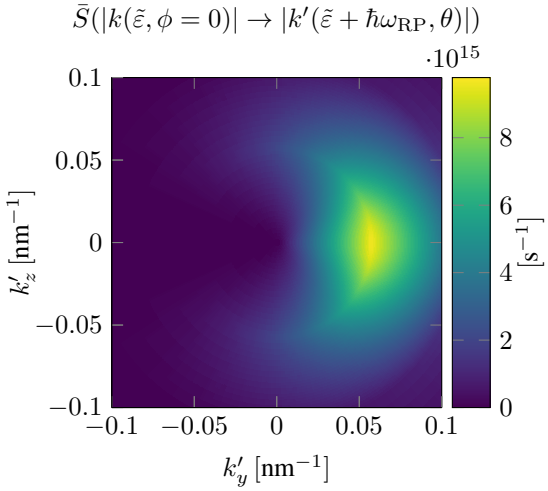

Fig. 8. RP Scattering rate of an electron in transport direction into all other possible states by absorption of a phonon.

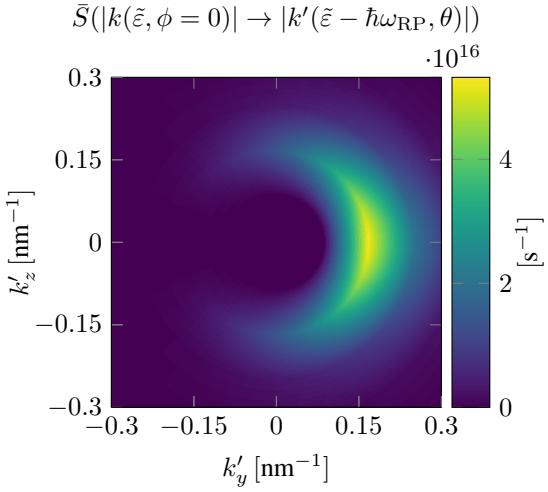

Fig. 9. RP Scattering rate of an electron in transport direction into all other possible states by emission of a phonon.

References

[1] "The nobel prize in physics 2010." "http://www.nobelprize.org/nobel_prizes/physics/laureates/2010/".

[2] "Graphene flagship is a future and emerging technology flagship by the european commission." "http://graphene-flagship.eu".

[3] A. Gnudi, D. Ventura, G. Baccarani, and F. Odeh, "Two-dimensional MOSFET simulation by means of a multidimensional spherical harmonics expansion of the Boltzmann transport equation," vol. 36, no. 4, pp. 575 – 581, 1993.

[4] S.-M. Hong, A. T. Pham, and C. Jungemann, *Deterministic solvers for the Boltzmann transport equation*. Computational Microelectronics, Wien, New York: Springer, 2011.

[5] D. Ruić and C. Jungemann, "A self-consistent solution of the Poisson, Schrödinger and Boltzmann equations by a full Newton-Raphson approach for nanoscale semiconductor devices," in *Simulation of Semiconductor Processes and Devices (SISPAD), 2013 International Conference on*, pp. 356–359, Sept 2013.

[6] Z. Kargar, D. Ruić, and C. Jungemann, "A Self-consistent Solution of the Poisson, Schrödinger and Boltzmann Equations for GaAs Devices by a Deterministic Solver," in *Simulation of Semiconductor Processes and Devices (SISPAD), 2015 International Conference on*, pp. 361–364, IEEE, 2015.

[7] T. Ando, "Theory of electronic states and transport in carbon nanotubes," *Journal of the Physical Society of Japan*, vol. 74, no. 3, pp. 777–817, 2005.

[8] M. Bresciani, A. Paussa, P. Palestri, D. Esseni, and L. Selmi, "Low-field mobility and high-field drift velocity in graphene nanoribbons and graphene bilayers," in *Electron Devices Meeting (IEDM), 2010 IEEE International*, pp. 32.1.1–32.1.4, Dec 2010.

[9] C. Jungemann, A.-T. Pham, B. Meinerzhagen, C. Ringhofer, and M. Bollhöfer, "Stable discretization of the Boltzmann equation based on spherical harmonics, box integration, and a maximum entropy dissipation principle," vol. 100, pp. 024502–1–13, 2006.

[10] E. H. Hwang and S. Das Sarma, "Acoustic phonon scattering limited carrier mobility in two-dimensional extrinsic graphene," *Phys. Rev. B*, vol. 77, 2008.

[11] R. S. Shishir, F. Chen, J. Xia, N. J. Tao, and D. K. Ferry, "Room temperature carrier transport in graphene," *Journal of Computational Electronics*, vol. 8, no. 2, 2009.

[12] S. Fratini and F. Guinea, "Substrate-limited electron dynamics in graphene," *Phys. Rev. B*, vol. 77, 2008.

[13] A. H. Castro Neto, F. Guinea, N. M. R. Peres, K. S. Novoselov, and A. K. Geim, "The electronic properties of graphene," *Rev. Mod. Phys.*, vol. 81, pp. 109–162, Jan 2009.

[14] T. Ando, T. Nakanishi, and R. Saito, "Berry's phase and absence of back scattering in carbon nanotubes," *Journal of the Physical Society of Japan*, vol. 67, no. 8, 1998.

[15] H. K. Gummel, "A self-consistent iterative scheme for one-dimensional steady state transistor calculations," pp. 455–465, October 1964.